

pubs.acs.org/est Article

Mechanistic Insight into the Reactivities of Aqueous-Phase Singlet Oxygen with Organic Compounds

Benjamin Barrios, Benjamin Mohrhardt, Paul V. Doskey, and Daisuke Minakata*



Cite This: https://doi.org/10.1021/acs.est.1c01712



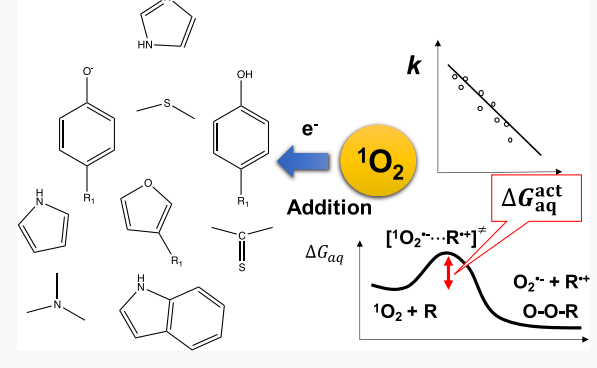
ACCESS

III Metrics & More

Article Recommendations

Supporting Information

ABSTRACT: Singlet oxygen ($^{1}O_{2}$) is a selective reactive oxygen species that plays a key role for the fate of various organic compounds in the aquatic environment under sunlight irradiation, engineered water oxidation systems, atmospheric water droplets, and biomedical systems. While the initial rate-determining charge-transfer reaction mechanisms and kinetics of $^{1}O_{2}$ have been studied extensively, no comprehensive studies have been performed to elucidate the reaction mechanisms with organic compounds that have various functional groups. In this study, we use density functional theory calculations to determine elementary reaction mechanisms with a wide variety of organic compounds. The theoretically calculated aqueous-phase free energies of activation of single electron transfer and $^{1}O_{2}$ addition reactions are compared to the experimentally determined rate constants in the literature to determine



linear free-energy relationships. The theoretically calculated free energies of activation for the groups of phenolates and phenols show excellent correlations with the Hammett constants that accept electron densities by through-resonance. The dominant elementary reaction mechanism is discussed for each group of compounds. As a practical implication, we demonstrate the fate of environmentally relevant organic compounds induced by photochemically produced intermediate species at different pH and evaluate the impact of predicting rate constants to the half-life.

KEYWORDS: singlet oxygen, photochemically produced intermediate species, reaction rate constants, linear free-energy relationships, fate of organic contaminant, aqueous phase

■ INTRODUCTION

Singlet oxygen, ${}^{1}O_{2}$ (${}^{1}\Delta_{g}$), is an important reactive oxygen species in the aquatic environment under sunlight irradiation, engineered water oxidation systems,2 atmospheric water droplets,³ and biomedical systems.⁴ It is the first electronically excited state of triplet-state molecular oxygen (${}^{3}O_{2}$, ${}^{3}\sum_{\sigma}$) at the ground state. 5-7 In the aquatic environment, ${}^{7}O_{2}$ is produced by photosensitizers like chromophoric dissolved organic matter (DOM). The lifetime of ¹O₂ in water is approximately 2-4 μ s resulting from the nonradiative and radiative solvent-dependent deactivation.^{7,8} While some argue that this short lifetime makes ${}^{1}O_{2}$ insignificant, 9,10 others believe that high levels of ${}^{1}O_{2}$ (e.g., $10^{-14}-10^{-11}$ M) make it an important reactant in the fate of numerous chemical and biological species. 11,12 The selective reactivity of $^{1}O_{2}$ may be useful without interfering with background DOM in oxidation and disinfection processes. ^{13,14} In the atmosphere, ¹O₂ plays a significant role as an oxidant in photochemical air pollution by converting nitric oxide to nitrogen dioxide. 15 In the human cell, reactive oxygen intermediates including ¹O₂ play diverse roles in inflammation, host defense, and homeostasis during damage caused by reactive oxygen species.¹⁶

While the initial rate-determining charge-transfer reaction mechanisms and kinetics of ¹O₂ have been extensively studied and documented for alkenes, 17,18 elementary reaction mechanisms with multiple-functional group organic compounds have not been elucidated yet due to difficulties in quantifying the resultant intermediates (e.g., superoxide anion radical¹⁹) and products.^{20,21} Many environmentally relevant contaminants are structurally diverse chemicals with multiple-functional groups, and identifying the dominant elementary reaction mechanism will help predict the reaction product(s) in the subsequent reactions. The ¹O₂ (standard reduction potential of 0.81 ± 0.02 V vs standard hydrogen electrode (SHE))²² is a highly selective electrophile that exclusively reacts with unsaturated organic compounds via (1) electrophilic addition (e.g., 1,2-, ene, and/or Diels-Alder reactions);²³ (2) dissociated oxygen via outer-sphere-type single

Received: March 15, 2021 Revised: May 19, 2021 Accepted: May 20, 2021



Scheme 1. Postulated Reaction Mechanisms of ¹O₂

electron transfer (SET); and (3) addition to heteroatoms (e.g., sulfur and nitrogen).²⁴ Each elementary reaction has been studied for single-functional group compounds, and the reaction mechanisms are well understood. For example, the use of the Rehm-Weller equation²⁵ has been used to determine the charge-transfer kinetics expected for full electron transfer for the reaction of 1O2 with phenols in organic solvents.²⁰ The other studies included ¹O₂ addition to phenol²¹ and the benzene ring of isoproturon.²⁶ The observed second-order rate constants, k, for phenolates and phenols range from 10^7 to 10^8 M⁻¹ s⁻¹ and 10^6 to 10^7 M⁻¹ s⁻¹, respectively 27,28 (Figure S1 for the compilation of k values in the Supporting Information (SI)). Addition to the sulfur atom of sulfides was determined to produce a sulfoxide with k values of 10^6-10^8 M⁻¹ s⁻¹. ^{29,30} Yet, it is not clear which reaction mechanism is dominant for reactions with ¹O₂ for compounds that have multiple potential reactive sites. Thus, challenges still present in experimentally identifying dominant rate-determining steps when multiple elementary reactions compete in a given molecule.31,32

Quantitative structure-activity relationships (QSARs) are useful approaches for predicting the reactivities of oxidants with organic compounds that have a wide variety of functional groups.³³ QSARs developed in previous studies to predict k values for ¹O₂ reactions used (1) half-wave potentials for phenols and anilines,³⁴ (2) one-electron oxidation/reduction potentials for phenolates and phenols,³⁵ (3) ionization potentials and energies of the highest occupied molecular orbitals (HOMOs) for aliphatic amines and aromatic compounds, 36-38 and (4) Hammett constants for phenolates and phenols.³⁹ These parameters represent the thermodynamic properties of organic compounds with various functional groups that can be correlated with experimentally determined k values. The reasonable correlations based on the half-wave potentials or one-electron oxidation potentials and the less steep slopes of these lines than those by the Rehm-Weller or Marcus equations indicate that the initial formation of a precursor complex with a small amount of charge transfer is the rate-determining step.³⁹ Given that the oxidation potential is related to the electron density of an organic compound, a similar correlation is expected for the addition of ¹O₂ to the ring of phenolates or phenols. While reasonable correlations were observed with the thermodynamic properties, the studies did not investigate parameters that represent the kinetics.

Density functional theory (DFT)-based quantum mechanical (QM) calculations 40,41 using solvation models 42 are a useful approach for investigating the reaction kinetics and thermodynamics of aqueous-phase radical-involved fast reactions. DFT calculations have been used to provide complementary information for experimentally observed reactions and to provide mechanistic insight into the reaction mechanisms. 43-45 Direct calculation of the aqueous-phase rate

constants, k, has been limited to small organic compounds given the large computational power required to obtain reliable barrier energies. Direct estimates of rate constants within experimental error (e.g., difference of a factor of 2) would require an accuracy within ± 0.5 kcal/mol of the free energies of activation based on transition-state theory. Thus, linear free-energy relationships (LFERs) were developed to relate the experimental k to the theoretically calculated free energies of activation using an implicit solvation model for reactive oxygen and halogen species. The SET reaction by sulfate radicals was also investigated using Marcus theory based on the free energies of reaction. The LFERs are useful for investigating the relative impact of various functional groups of a given structure on the rate constants. Accuracies for rate constant predictions were within a factor of 5 of the experimental values. The structure of the structure of 5 of the experimental values.

In this study, we use DFT calculations to determine elementary reaction mechanisms embedded in the aqueousphase ¹O₂ reactions with a wide variety of organic compounds. The functional groups investigated in this study are found in the structures of environmentally relevant contaminants, including phenolates/phenols, furans, aromatic and aliphatic amines, sulfides, imidazoles, thioureas, pyrroles, and indoles. The alkenes are excluded because of the known mechanisms. Marcus theory and statistical thermodynamics are used to determine the kinetic properties of single electron transfer and ¹O₂ addition reactions. We compare the theoretically calculated aqueous-phase free energies of activation to the experimentally determined k values in the literature to determine the LFERs. The dominant elementary reaction is discussed in each group of compounds. The determination of kvalues enables prediction of the fate of environmentally relevant organic compounds induced by photochemically produced intermediate species. Thus, as a practical implication, we demonstrate the fate of representative compounds based on the predicted k values at different pH and evaluate the impact of predicting rate constants on the half-life.

MATERIALS AND METHODS

The postulated mechanism of ${}^{1}O_{2}$ with organic compounds is shown in Scheme 1. When ${}^{1}O_{2}$ encounters the target organic compound, R, in the aqueous-phase diffusion process, ${}^{1}O_{2}/R$ forms a loosely bound complex without the proper conformation for the reaction to occur. The contact pair may either diffuse apart or find the proper orientation to reversibly form a precursor complex (i.e., $[{}^{1}O_{2}^{\bullet-}\cdots R^{\bullet+}])$ via charge transfer. The precursor complex follows two major reaction mechanisms: (1) SET via a transition state of $[{}^{1}O_{2}^{\bullet-}\cdots R^{\bullet+}]^{\neq}$ to form a superoxide anion radical, $O_{2}^{\bullet-}$, and a radical cation, $R^{\bullet+}$, and/or (2) the addition of ${}^{1}O_{2}$ via a transition state of $[O_{2}\cdots R]^{\neq}$ to form a product such as an endoperoxide (OOR).

Table 1. Thermodynamic and Kinetic Properties of Compounds Investigated in This Study, Marcus Theory Solvent Reorganization Energy and Imaginary Frequency Obtained for the Determination of Transition State of Free Energy of Activation for the Addition, and Experimentally Determined Literature-Reported Rate Constants, $k_{\rm exp}{}^a$

			•			-				
no.	name	pK_a	$\Delta G^{ m act}_{ m aq,SET} \ m (kcal/mol)$	$\Delta G^{ m react}_{ m aq,SET} \ m (kcal/mol)$	λ (kcal/mol)	$\Delta G^{ m act}_{ m aq,add} \ m (kcal/mol)$	imaginary frequency ^c (cm ⁻¹)	$\Delta G^{ ext{react}}_{ ext{aq,add}} (ext{kcal/mol})^d$	$(M^{-1} s^{-1})$	references for $k_{\rm exp}$
1	phenolate	10.0	2.0	-8.5	21.6	1.9	-253.2	-9.5	1.7×10^{8}	28 and 39
2	2-chlorophenolate	8.5	3.1	-5.6	22.0	1.6	-167.0	-7.4	1.6×10^{8}	35 and 39
3	2-methoxyphenolate	10.0	1.0	-13.6	23.1	0.5	-246.9	-10.4	4.4×10^{8}	39
4	2-methyl ester phenolate	9.8	4.9	-1.3	22.0	5.6	-273.9	-3.3	1.6×10^{8}	28
5	2-nitrophenolate	7.2	9.2	6.1	23.1	6.8	-274.5	6.8	3.2×10^7	35, 39, and 76
6	3-chlorophenolate	9.1	3.4	-4.3	21.4	1.9	-142.4	-8.6	1.1×10^{8}	35, 39, and 76
7	3-methoxyphenolate	9.6	1.9	-9.0	21.9	-0.7	-193.0	-14.6	2.8×10^{8}	35 and 39
8	3-methylphenolate	10.1	1.7	-9.4	21.7	1.0	-218.8	-11.9	2.0×10^{8}	35
9	3-nitrophenolate	8.3	5.3	0.0	21.4	3.1	-170.4	-0.3	3.9×10^{7}	35, 39, and 76
10	4-acetylphenolate	8.0	5.0	-0.8	21.3	6.5	-302.3	-3.7	2.4×10^{7}	39
11	4-chlorophenolate	9.4	2.4	-7.3	22.0	2.5	-260.3	-7.5	1.1×10^{8}	39, 76, and 77
12	4-cyanophenolate	8.0	5.9	1.4	20.7	7.4	-320.1	-1.3	6.2×10^{6}	39
13	4-methoxyphenolate	10.2	0.5	-17.0	23.8	-3.5	-211.0	-13.1	6.6×10^{8}	39
14	4-methylphenolate	10.3	1.1	-12.5	22.3	0.2	-220.8	-10.8	3.6×10^{8}	28 and 39
15	4-nitrophenolate	7.1	9.2	6.6	21.6	10.6	-344.8	2.1	4.1×10^{6}	28 and 39
16	4-tert-butylphenolate	10.4	1.1	-12.4	22.1	-0.6	-214.0	-12.5	3.6×10^{8}	39
17	2,4-dimethylphenolate	10.6	0.4	-16.6	22.3	-1.0	-227.4	-13.0	3.5×10^{8}	35
18	2,4-dichlorophenolate	7.9	3.6	-4.3	22.3	1.9	-158.9	-8.9	1.5×10^{8}	28 and 39
19	2,6-dimethylphenolate	10.6	0.8	-13.6	22.0	-2.5	-134.1	-13.0	2.0×10^{8}	35
20	4-hydroxyphenolate	9.8	0.5	-16.7	23.9	-2.8	-226.5	-12.3	5.6×10^{7}	78
21	2,6-dimethoxyphenolate	10.0	0.9	-14.6	23.6	-1.6	-143.3	-11.8	8.7×10^{8}	28
22	3-methyl-4-chlorophenolate	9.5	2.1	-8.4	22.0	1.6	-247.2	-10.8	1.3×10^{8}	35
23	2,3,5-trichlorophenolate	6.6	6.6	2.1	21.8	3.4	-221.7	-4.7	4.3×10^6	35
24	2,4,6-trimethylphenolate	11.1	0.3	-17.3	22.6	-3.5	-129.6	-14.3	6.0×10^{8}	35
25	2,4,6-tribromophenolate	6.8	4.5	-2.1	22.1	3.3	-210.0	-8.6	8.3×10^7	35
26	2,4,6-trichlorophenolate	6.2	5.0	-2.1 -1.4	22.6	3.2	-210.0	-5.2	1.4×10^8	28 and 39
27	4-bromophenolate	9.2	2.6	-1. 4 -6.7	21.7	1.2	-106.2	-12.9	1.4×10^{8} 1.5×10^{8}	79
28	2,6-dimethyl-4- bromophenolate	10.1	1.2	-0.7 -11.9	22.2	-0.3	-183.9	-15.3	3.9×10^8	79
29	2,4-dinitrophenolate	4.1	18.9	18.8	22.5	14.2	-0.1	11.2	4.1×10^{5}	39
30	4-fluorophenolate	9.9	1.9	-9.7	22.7	0.8	-236.3	-9.2	3.5×10^{8}	77
31	2-nitro-4-chlorophenolate	6.5	9.7	6.7	23.6	7.4	-230.3 -281.1	0.1	2.1×10^7	80
32	4,6-dinitro-2-	4.7	16.2	15.6	23.1	13.4	-281.1 -370.3	14.2	1.3×10^5	39
33	methylphenolate 2,6-dinitro-4-	4.2	13.1	11.5	23.6	0.0	-89.4	12.2	1.4×10^{7}	39
	methylphenolate								7	
34	tyrosine	9.1	1.1	-12.4	22.1	0.0	-236.6	-10.8	5.2×10^{7}	81
35	glycyl-tyrosine	2.9, 9.1, 9.6	1.2	-11.8	22.0	1.2	-239.3	-11.3	1.9×10^{7}	81
36	glycyl-tyrosyl-alanine	3.3, 9.1, 9.6	1.6	-10.1	22.0	2.5	-247.9	-8.1	1.0×10^{8}	82
37	tyrosyl-glycine	2.3, 9.1	0.8	-13.5	22.2	-4.8	-278.0	-10.8	4.3×10^{7}	81
38	tyramine	10.4, 9.6	1.2	-11.9	22.1	0.7	-240.0	-10.3	2.3×10^{8}	83
39	phenol	10.0	23.0	23.0	24.3	14.4	-359.0	0.8	7.9×10^{6}	39, 84, and 85
40	2-chlorophenol	8.5	27.5	27.4	24.5	16.6	-378.6	0.9	9.1×10^{6}	39
41	2-methoxyphenol	10.0	43.5	14.8	25.5	12.8	-337.8	-2.2	6.0×10^{6}	39
42	2-methyl ester phenol	9.8	27.2	27.1	24.7	16.2	-366.6	3.2	2.0×10^{6}	28
43	2-nitrophenol	7.2	35.2	34.2	24.4	19.1	-380.8	5.5	1.3×10^{6}	39
44	3-chlorophenol	9.1	27.0	26.9	24.3	16.1	-369.2	2.1	3.3×10^6	39
45	3-methoxyphenol	9.6	17.8	17.3	24.4	11.7	-325.4	-1.0	1.3×10^7	39
46	3-methylphenol	10.1	21.0	20.9	24.7	13.1	-339.2	-0.3	1.8×10^{7}	35
47	1,3-benzenediol-4-chloro	8.3	21.4	21.3	24.7	14.9	-344.2	4.0	2.1×10^{7}	84
48	1,4-benzenediol-chloro	9.2	16.7	15.7	26.1	11.0	-292.0	-1.3	1.7×10^7	84
40	1,T-Delizelledioi-Ciliofo	7.4	10./	13./	20.1	11.0	-474.0	-1.5	1./ ^ 10	OT

Table 1. continued

no.	name	pK_a	$\Delta G^{ m act}_{ m aq,SET} \ m (kcal/mol)$	$\frac{\Delta G^{\mathrm{react}}}{\mathrm{(kcal/mol)}}$	λ (kcal/mol)	$\Delta G^{ m act}_{ m aq,add} \ m (kcal/mol)$	imaginary frequency ^c (cm ⁻¹)	$\Delta G^{ m react}_{ m aq,add} \ (m kcal/mol)^d$	$(M^{-1} s^{-1})$	references for $k_{\rm exp}$
49	1,3-benzenediol	9.3, 9.8	19.7	19.4	24.4	12.4	-333.3	0.8	2.0×10^{7}	84
50	3-nitrophenol	8.3	33.3	32.6	24.4	18.2	-373.6	4.2	2.8×10^{6}	35
51	1,4-dihydroxybenzene	9.8	13.3	11.2	26.1	8.8	-273.1	-1.8	3.8×10^{7}	39
52	4-acetylphenol	8.1	30.3	29.9	24.0	18.9	-378.1	6.5	1.5×10^{6}	39
53	4-chlorophenol	9.4	23.6	23.6	24.9	15.2	-358.0	3.3	6.0×10^{6}	39
54	4-cyanophenol	8.0	33.1	32.3	23.5	21.2	-398.7	11.1	2.4×10^{5}	39
55	4-methoxyphenol	10.2	12.6	10.2	26.0	9.1	-274.7	9.1	1.7×10^{7}	39
56	4-methylphenol	10.3	17.6	17.0	24.8	11.3	-306.6	-1.4	7.3×10^6	39
57	4-nitrophenol	7.1	40.0	37.9	23.7	22.3	-393.2	11.7	2.6×10^{5}	39
58	4-tert-butylphenol	10.4	18.8	18.4	24.7	12.0	-284.3	-2.9	1.2×10^{7}	39
59	2,4-dimethylphenol	10.6	16.3	15.5	24.8	10.1	-288.8	-3.8	2.3×10^{6}	35
60	2,4-dichlorophenol	7.9	28.3	28.2	25.0	17.1	-370.3	3.5	2.8×10^{6}	39
61	2,6-dimethylphenol	10.6	18.2	17.8	24.5	11.9	-373.1	-3.1	5.1×10^6	35
62	2,6-dimethoxyphenol	10.0	16.7	15.7	25.7	13.0	-335.0	-3.2	3.6×10^{7}	39
63	3-methyl-4-chlorophenol	9.5	21.5	21.4	24.8	14.2	-337.0	1.7	3.0×10^{7}	35
64	2,3,5-trichlorophenol	6.6	36.8	35.6	24.4	18.5	-341.6	1.5	1.5×10^{5}	35
65	2,4,6-trimethylphenol	11.1	14.1	12.5	24.9	9.5	-389.3	-5.2	3.2×10^6	35
66	2,4,6-tribromophenol	6.8	36.6	35.4	24.3	20.2	-274.0	4.1	2.7×10^6	35
67	2,4,6-trichlorophenol	6.2	32.0	31.6	25.0	18.9	-389.7	4.0	1.7×10^{7}	39
68	pentachlorophenol	4.7	55.8	49.1	23.9	20.8	-377.3	2.2	2.0×10^{5}	39
69	3,4-dihydroxyphenylalanine	9.1	18.3	17.6	25.9	12.9	-300.0	2.5	9.0×10^{8}	86
70	2-methylfuran	-2.6	16.7	16.0	24.2	1.2	-290.3	-25.3	6.0×10^{7}	87
71	2,5-dimethylfuran	-2.7	11.5	9.1	24.6	-0.5	-246.2	-27.4	1.2×10^9	28, 88, and 89
72	furfuryl alcohol	9.6	19.8	19.2	26.8	3.5	-291.5	-24.4	1.1×10^{8}	90
73	N,N-dimethyl-4- nitrosoaniline	-0.9	10.5	5.4	30.5	15.2	-411.3	-25.3	5.6×10^{7}	91 and 92
74	<i>N,N,N,N</i> -tetramethyl- <i>p</i> -phenylenediamine	5.9	1.3	-17.0	29.5	6.7	-303.3	-27.4	3.3×10^9	88
75	2-dimethylamino-5,6- dimethylpyrimidin-4-ol	4.3	13.8	12.4	24.0	6.0	-145.5	-24.4	9.0×10^{7}	93
76	methionine	2.3, 9.2	27.7	26.4	40.6	6.2	-178.2	11.5	4.0×10^{7}	82, 94, and 95
77	diethyl sulfide	n.a. ^b	20.5	20.5	21.1	5.7	-71.3	5.6	1.8×10^{7}	28
78	glycyl-methionine	2.3, 9.6	21.8	21.8	21.9			4.2	1.3×10^{7}	82
79	methionine methyl ester	10.7	31.8	31.4	24.7	6.9	-234.2	13.4	7.0×10^6	82
80	histamine	5.8, 9.4	21.7	21.6	24.6	3.7	-180.4	-17.4	1.1×10^{8}	
81	histidyl-glycine	3.3, 7.8	24.1	24.0	27.6	6.6	-222.8	-12.4	6.6×10^{7}	82
82	histidine	1.8, 6.0, 9.2	21.8	21.6	26.0	5.9	-326.3	-13.7	6.1×10^7	82
83	glycyl-histidine	3.3, 8.2	18.2	17.6	25.5	4.0	-183.5	-17.6	8.3×10^{7}	82
84	imidazole	6.8	23.4	23.4	24.5	5.3	-314.2	-16.4	3.6×10^{7}	87, 91, and 94
85	thiourea	13.9	20.3	20.3	21.8	6.0	-31.6	-8.0	4.4×10^{6}	94
86	allyl-thiourea	14.6	19.6	19.5	21.8	6.3	-49.0	-7.2	4.0×10^{6}	94
87	methyl-thiourea	15	19.2	19.1	21.7	9.6	-27.7	-8.0	2.0×10^{6}	94
88	pyrrole	16.5	14.1	12.9	23.4	1.0	-176.5	-16.4	5.0×10^{8}	96
89	3-cyanopyrrole	14.6	24.6	24.6	23.6	6.2	-306.6	-11.1	3.4×10^{7}	96
90	3-phenylpyrrole	16.7	11.6	9.5	23.3	0.7	-138.3	-17.3	7.9×10^{8}	96
91	2,2,6,6-tetramethylpiperidin- 4 -ol e	9.9	13.8	9.4	33.6				4.0×10^{7}	97
92	1,4-diazabicyclo[2.2.2] octane e	8.8	4.8	-5.2	28.6				2.8×10^{8}	97
93	alanine	2.3, 9.7	15.2	6.3	47.6	15.2	47.6	14.6	3.0×10^{7}	78
94	indole-3-carboxylate ion	3.5	13.4	11.9	23.9	8.5	-246.0	15.4	1.4×10^{7}	82
95	indole-3-butyrate ion	4.7	9.8	6.6	24.0	3.9	-260.6	-23.5	7.2×10^{7}	82
96	indole-3-propionate ion	4.8	9.9	6.7	24.1	4.6	-249.7	-23.6	7.3×10^7	82
97	indole-3-acetate ion	4.7	8.8	4.3	25.8	3.7	-219.8	-24.2	9.2×10^{7}	82
98	indole-3-acetic acid	4.7	11.2	8.6	24.7	5.2	-289.8	-22.8	2.0×10^{7}	76
99	indole	16.2	13.5	12.1	23.7	7.0	-322.8	-19.1	7.0×10^{7}	98
100	tryptophan	2.8, 9.4	11.7	7.5	29.9	4.4	-178.1	-17.8	2.6×10^7	78

Table 1. continued

^aAll of the free energies were calculated at 298 K. ^bn.a.: the p K_a value is not available. ^cImaginary frequencies obtained at the M06-2X/cc-pVDZ level with the SMD solvation model. ^{e1}O₂ addition was not accounted as discussed in the main text.

To study each reaction step, we used the following theories and QM methods. We calculated the diffusion rate constant, k_D, using Smoluchowski's equation⁵⁴ and diffusion coefficients using the Hayduk-Laudie or Nernst equation (Text S1 in the SI). The experimentally obtained rate constants, k_{exp} , were modified by subtracting the contribution of k_D . The reaction rate constant resulting from the chemical reaction, k_{chem} , was obtained using the Collins-Kimball theory.⁵⁵ We used Spartan'18⁵⁶ to search the conformers of a precursor complex composed of ¹O₂ and a target organic compound using a modified Merck molecular force field (MMFF) method⁵⁷ and the modified intrinsic reaction coordinate (IRC) method. Once the precursor complex was found, a single-point energy calculation was performed to determine the aqueous-phase interaction energy, $\Delta E^{\rm int}_{\rm aq}$. The detailed procedure is provided in Text S2 in the SI.

The SET reaction mechanism is categorized into three groups: (1) outer sphere, (2) inner sphere, and (3) interior. The SET reaction of $^1{\rm O}_2$ with an organic compound is not a barrierless interior reaction. Thus, we used Marcus theory to calculate the aqueous-phase free energy of activation, $\Delta G^{\rm act}_{\rm aq,SET}$, in eq 1 as no bond cleavage is involved in the SET reaction of $^1{\rm O}_2$ (i.e., dissociative electron transfer). The detailed method to calculate the $\Delta G^{\rm act}_{\rm aq,SET}$ and free energy of reaction, $\Delta G^{\rm react}_{\rm aq,SET}$, values and the inner- and outer-sphere reorganization energies, λ , and the method validation with experimental observation are given in Text S3 in the SI. It should be noted that the accurate estimation of the λ values from both inner- and outer-sphere reorganizations is critical for the estimation of the $\Delta G^{\rm act}_{\rm aq,SET}$ values

$$\Delta G^{\text{act}}_{\text{aq,SET}} = \left(\lambda + \Delta G^{\text{react}}_{\text{aq,SET}}\right)^2 / 4\lambda$$
 (1)

The $\Delta G^{\text{act}}_{\text{aq,add}}$ value for the addition of $^{1}\text{O}_{2}$ was obtained based on

$$\Delta G^{\text{act}}_{\text{aq,add}} = \Delta G^{\text{act}}_{\text{gas,add}} + \Delta G^{\text{act}}_{\text{solv,add}}$$
(2)

where $\Delta G^{\rm act}_{\rm aq,add}$ was obtained by subtracting the aqueousphase free energies of reactants from the free energy of the transition state at a standard temperature of 298 K, $\Delta G_{\text{gas,add}}^{\text{act}}$ is the gaseous phase free energy of activation, and $\Delta G_{
m solv,add}^{
m gashad}$ is the free energy of solvation. Unrestricted exchangecorrelation functional, UM06-2X/cc-pVDZ, 61 in combination with the universal solvation model, which was based on the solute electron density (SMD),62 was used to calculate the wave function for given molecular and radical structures in the aqueous phase. The unrestricted DFT (UDFT) performed well in comparison to multireference methods for deriving energies and geometries of the singlet biradical.⁶³ Employing hybrid DFT further enhanced the accuracy of the UDFT in describing the biradical system.⁶⁴ UM06-2X hybrid DFT was successfully used for the investigation of the 1O2 reaction with phenol in the aqueous phase.²¹ Once the structural optimization was completed, a single-point energy calculation at the level of UM06-2X/Aug-cc-pVTZ was conducted to obtain reliable energies. In the spin-unrestricted calculation, broken symmetry was used and special attention was paid to

the spin contamination. To correct the electronic energy resulting from the spin contamination, we used an approximate spin-projection method. 64,65 The basis set superposition error was corrected by a counterpoise method. 66 In addition, the solvent cage effect⁶⁷ and tunneling effect⁶⁸ were accounted for in the bimolecular reactions. Text S4 in the SI provides the detailed procedure to calculate the $\Delta G^{
m act}_{
m aq,add}$ values, the benchmark calculation with the single-point energy calculation using CCSD(T), and the method validation with experimental values. We did not intend to obtain the absolute energy values of each reaction as this is computationally demanding and prohibitive in obtaining accurate values for the aqueous phase; however, we obtained the relative energies that were sufficiently accurate to evaluate the impact of various structures and functional groups under the same reaction mechanism. All electronic structural calculations were performed using Gaussian 16,69 with the exception of a coupled-cluster method that was used for the benchmark calculation with Molpro. 70 All calculations were performed with the Michigan Tech highperformance cluster "Superior" and house-made workstations.

The $\Delta G^{\rm act}_{\rm aq}$ values were used to determine LFERs for each reaction mechanism (i.e., SET or $^{1}{\rm O}_{2}$ addition). Assuming that an elementary reaction proceeds by the same reaction mechanism, the log of the rate constant and the log of the equilibrium constant are linearly related. According to the transition-state theory, the log of the rate constant and the free energy of activation are linearly related. Combining these two concepts enables the development of the LFER shown in eq 3, although the empirically established LFERs and the assumption hold for specific reactions 4.5

$$\ln k_{\rm chem} = -\rho \Delta G^{\rm act}_{\rm aq} + \sigma \tag{3}$$

where ρ is a coefficient for the free energy of activation that accounts for the transmission coefficient and the frequency of the transition state to form products, and σ is a coefficient expressed in kcal/mol. We determined various transition states for each elementary reaction and calculated the $\Delta G^{\rm act}_{\ \ aq}$ values using UM06-2X/cc-pVDZ and the SMD solvation model. Once we determined the transition state that provided the smallest $\Delta G^{\rm act}_{\ aq}$ value, we performed the single-point energy calculation using UM06-2X/Aug-cc-pVTZ to calculate the $\Delta G^{\rm act}_{\ aq}$ value for the development of LFER.

■ RESULTS AND DISCUSSION

Overall Results. A total of 100 organic compounds was investigated for the determination of LFERs including 38 phenolates (compound nos. 1–38 in Table 1), 31 phenols (nos. 39–69), 3 furan derivatives (nos. 70–72), 3 aromatic amines (nos. 73–75), 4 sulfides (nos. 76–79), 5 imidazole derivatives (nos. 80–84), 3 thiourea derivatives (nos. 85–87), 3 pyrrole derivatives (nos. 88–90), 3 aliphatic amines (nos. 91–93), and 7 indole derivatives (nos. 94–100). The organic compounds cover a wide range of functional groups, with $k_{\rm exp}$ values ranging from 10^5 to 10^9 M $^{-1}$ s $^{-1}$ (see Figure S1 for a box plot in the SI and Text S5 for the critical data evaluation). Table 1 includes the $k_{\rm exp}$ values in the literature and our theoretically calculated $\Delta G^{\rm act}_{\rm aq,SET}$, $\Delta G^{\rm react}_{\rm aq,SET}$, λ , $\Delta G^{\rm act}_{\rm aq,add}$,

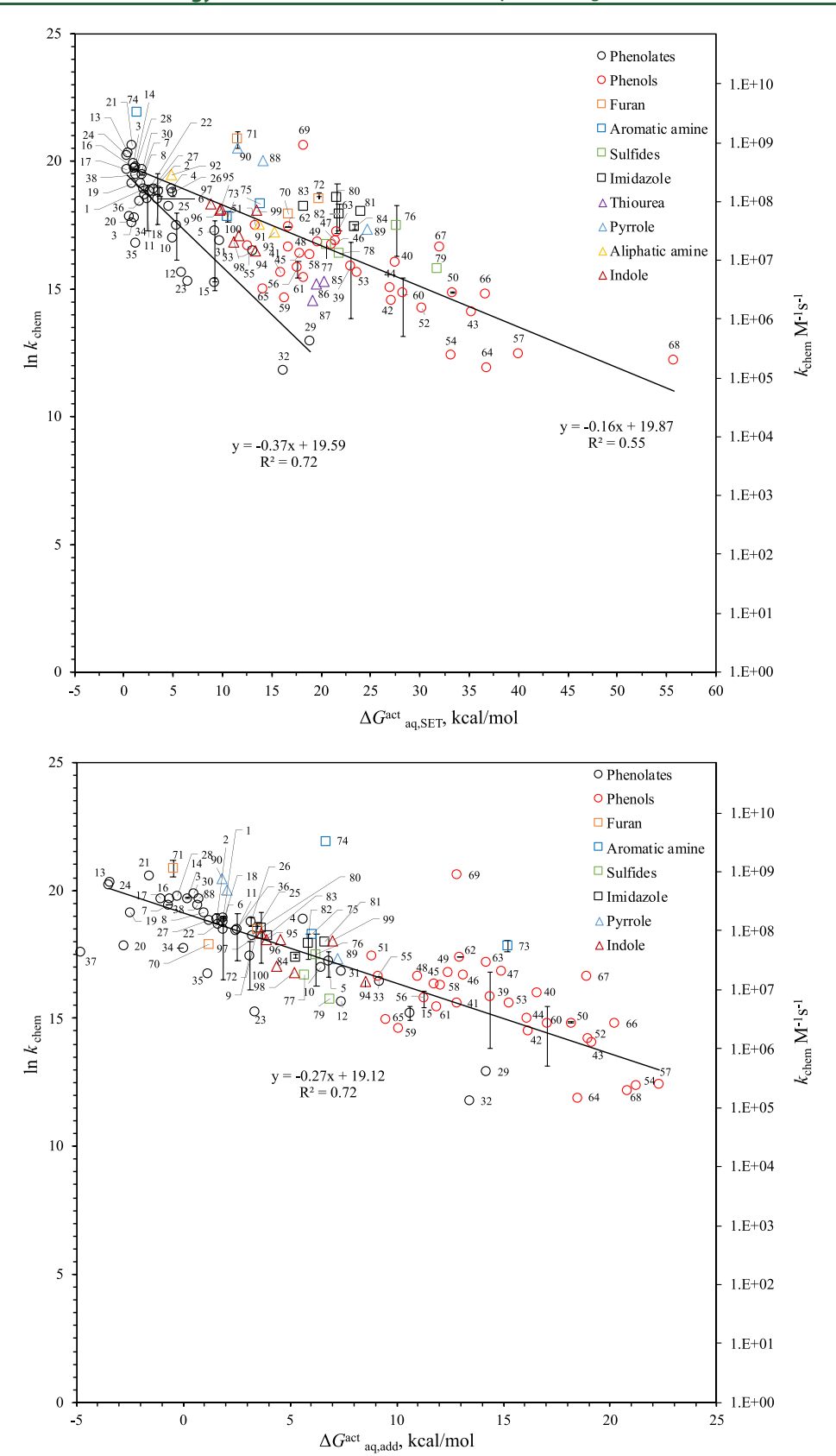


Figure 1. Linear free-energy relationships between chemical reaction rate constants and theoretically calculated free energies of activation for the aqueous-phase ${}^{1}O_{2}$ reaction undergoing SET (top) and addition (bottom). The error bar represents the range of k_{chem} values calculated from the reported experimentally determined values. Compounds (nos. 20, 37, and 69) were not included in both LFERs, and compounds (nos. 73, 74, 91, and 92) were not included in LFER for addition (see the text for the detailed reasons).

imaginary frequency, $\Delta G^{\rm react}_{\rm aq,add}$, and values for the development of LFERs. Tables S2 and S3 in the SI include all of the values used for the corrections and additional information and other transition states that were identified.

The plot of $\ln k_{\rm chem}$ against the $\Delta E^{\rm int}_{\rm aq}$ values does not show a strong correlation except for phenolates (Figure S3 in the SI), indicating that the $\Delta E_{\text{aq}}^{\text{int}}$ values that were determined based on the energy minimum of a precursor complex are not the rate-determining step for the group of phenols and other compounds. In contrast, the Rehm-Weller-type plot (Text S6 and Figure S4 in the SI) for phenolates shows that the charge separation step is the rate-determining step. Our plot contains extensive data and is consistent with the observation for the limited number of data by other studies. 20,99,100 We also calculated the distribution of charges on the precursor complexes using natural bond orbital analysis. 99 A reasonable correlation was found between $\ln k_{\mathrm{chem}}$ and the total charge of ¹O₂ for each precursor complex of both groups of phenolates and phenols (Figure S5 in the SI). The findings support that the charge transfer is the key rate-determining step. The $k_{\rm exp}$ values are smaller than the diffusion-limited rate constants, $k_{\rm D}$ $(\sim 1.1 \times 10^{10} \text{ M}^{-1} \text{ s}^{-1})$, by greater than an order of magnitude, and the approximated line does not appear to plateau and the quenching rate calculated by the Rehm-Weller's equation is close to a diffusion limit in the exergonic region ($\Delta G^{\text{react}}_{\text{aq,SET}}$ < 0 kcal/mol). We confirmed the limiting slope of -0.73 for $\ln k_{\rm chem}$ in the region where $\Delta G^{\rm react}_{\rm aq,SET}$ is greater than 5 kcal/mol and obtained a slope of -0.11 for the $\ln k_{\rm chem}$ values in the same region. The comparison of these two slopes represented approximately 15% of the charge transfer that was expected for complete electron transfer for the group of phenolates. Thomas and Foote reported 44% of charge transfer for the group of phenols for the quenching rate of ¹O₂ in an organic solvent,²⁰ and Saito et al. reported about 60% for N,Ndimethylanilines in a methanol-water solvent. 19 Although Saito et al. commented that the slope in the aqueous phase is larger than the slope in an organic solvent due to a more significant contribution of charge-transfer character, 19 our value appears to contradict their results. Possible reasons may include the scattering data with an $r^2 = 0.7$ that we collected from various experimental studies in the literature as compared to using one set of experiments for the same group of compounds. It should be noted that the estimation assumed a constant charge transfer over the whole series, which may result in an oversimplification of the estimated value.⁹⁹ As Schuster et al. observed, the slope does not necessarily represent the degree of charge transferred at the transition state. 100 Thus, we individually investigated the charge distribution on the precursor complex of ¹O₂ with phenolate using natural bond orbital theory. 99 As shown in Figure S5, the charge on ¹O₂ of precursor complexes with the group of phenolates ranged from -0.1 to -0.5, indicating that 10-50%of the original phenolate charge (i.e., -1.0) was separated upon the formation of those precursor complexes.

Figure 1 shows the LFERs in eq 3 for SET and 1O_2 addition reactions for all compounds investigated in this study. Overall, we found LFERs for both groups of phenolates and phenols via SET: $\ln k_{\rm chem} = -0.37 \Delta G^{\rm act}_{\rm aq,SET} + 19.59$ with $r^2 = 0.72$ for the group of phenolates and $\ln k_{\rm chem} = -0.16 \Delta G^{\rm act}_{\rm aq,SET} + 19.87$ with $r^2 = 0.55$ for the rest of compounds. For 1O_2 addition reactions, we determined LFER to be $\ln k_{\rm chem} = -0.27 \Delta G^{\rm act}_{\rm aq,add} + 19.12$ with $r^2 = 0.72$ for all of the compounds as all data followed a similar trend. The

compounds excluded in the analysis of LFERs include 4hydroxyphenolate (no. 20) and tyrosyl-glycine (no. 37) due to their significantly smaller k_{chem} values based on the functional groups (i.e., OH and alkyl amine) and probable experimental uncertainties and 3,4-dihydroxyphenylalanine (no. 69) due to the significantly larger $k_{\rm chem}$ value $(9.7 \times 10^8 \ {\rm M}^{-1} \ {\rm s}^{-1})$ compared to all other compounds. The sample deviations (SD) in eq 4 between the experimentally determined values, $k_{
m chem,exp}$, and calculated values, $k_{
m chem,calc}$, based on the LFER were 0.061 for SET and 0.084 for ¹O₂ addition, respectively, among phenolates (N = 36). The SD statistically indicates where the predicted data are distributed as compared to the experimental data under the assumption of a normal distribution. 49 Both LFERs estimate all of the k_{chem} values within the difference of a factor of 1.2 from the experimental value. Similarly, the SD value was 0.098 for ¹O₂ addition to phenols (N = 30) and the LFER estimates all of the k_{chem} values within the difference of a factor of 1.2 from the experimental value. The predictability of LFERs for the $k_{
m chem}$ values developed for the ${}^{1}O_{2}$ reactions in this study is superior to those previously developed for other reactive oxygen species such as hydroxyl radicals (e.g., difference of a factor of 2-5)^{50,51}

$$SD = \sqrt{\frac{1}{N-1} \sum_{i=1}^{N} \left(\frac{k_{\text{chem,exp}} - k_{\text{chem,calc}}}{k_{\text{chem,exp}}} \right)^2}$$
 (4)

A stronger correlation of the LFER for phenolate indicates that the extent of change in delocalization of the formal negative charge of the precursor complex by functional groups is proportional to the observed rate constants. Different slopes for the groups of phenolates and the rest of compounds indicate different mechanisms (see the section below for the discussion of reaction mechanisms). Notably, the phenolates with strong electron-withdrawing groups (i.e., cyano and nitro) were not included in the correlation between the $k_{\rm chem}$ values and the half-wave potentials by previous observation due to the inability of half-wave potentials to account for possible interaction of functional groups in the proximity position and the formation of potential internal hydrogen bonding. However, this does not apply to our $\Delta G^{\rm act}_{\rm aq,SET}$ values, which account for both inter- and intraelectrostatic interactions with the water solvent through hydrogen bonding.

For phenolates, the $\Delta G^{\rm act}_{\rm aq,SET}$ values ranged from 0.3 to 18.9 kcal/mol and those for $^{1}{\rm O}_{2}$ addition varied from -4.8 to 13.4 kcal/mol, indicating that phenolates undergo both SET and ¹O₂ addition reactions. For the majority of phenolates, the $\Delta G_{\text{aq}}^{\text{act}}$ values for SET and $^{1}\text{O}_{2}$ addition are very close, although direct comparisons are difficult due to the use of different theories for each mechanism and uncertainties attributed to each method. For phenols, the $\Delta G^{\rm act}_{\rm aq,SET}$ values ranged from 12.6 to 55.8 kcal/mol, while the $\Delta G^{\rm act}_{\rm aq,add}$ values ranged from 9.1 to 22.3 kcal/mol. It is problematic to compare these values for the same reason described above; however, it appears that all of the phenols primarily undergo ¹O₂ addition over SET. For other groups of compounds such as furan derivatives, aromatic amines, sulfides, and imidazole, pyrrole, and indole derivatives, ¹O₂ addition occurs preferably over SET with compound nos. 73, 74, 91, and 92 being the exceptions (see the detailed discussion in the section below). The one consistent correlation for all of the compounds investigated for ¹O₂ addition indicates a less important

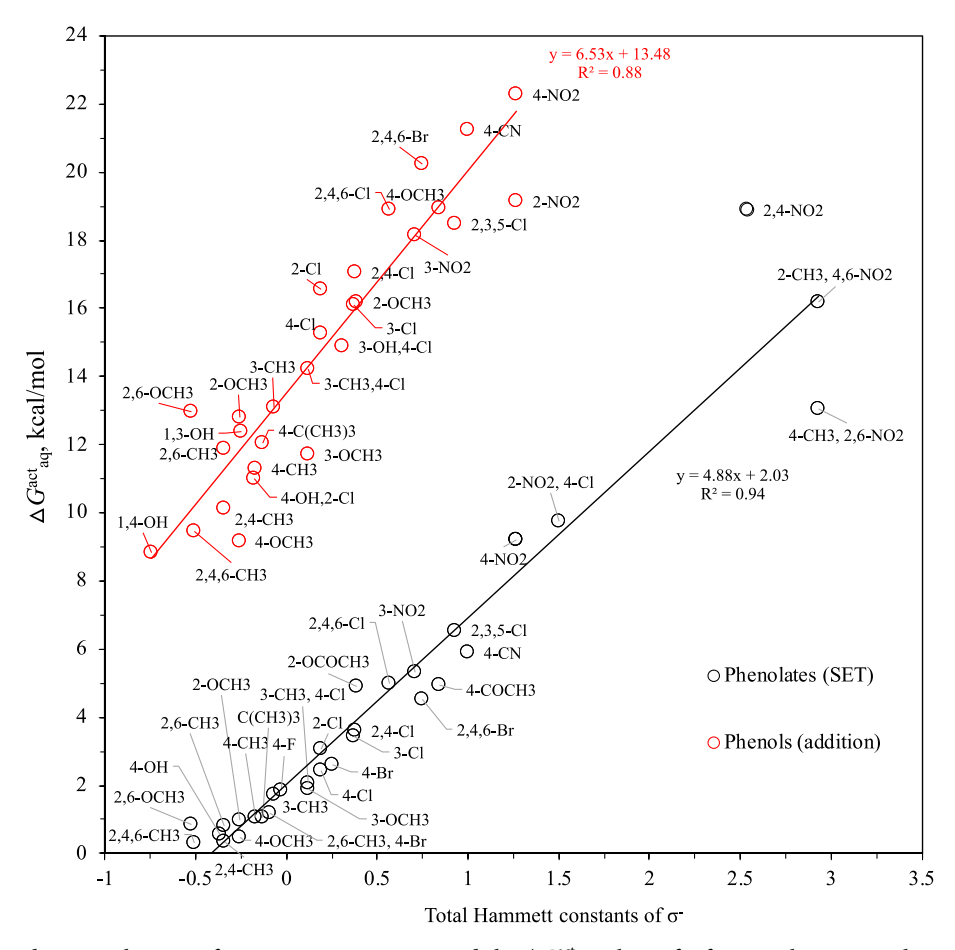


Figure 2. Relationships between the sum of Hammett constants σ^- and the $\Delta G^{\rm act}_{aq}$ values of a functional group on the group of phenolates for single electron transfer and phenols for $^1{\rm O}_2$ addition.

precursor formation and a consistent addition mechanism of ${}^{1}\mathrm{O}_{2}$ to the ring.

A recent observation of QSAR ($\log k_{\rm exp}$ vs half-wave function) for 37 phenolates reports the following correlation, $\log k_{\rm exp} = 2.46E_1 + 9.89$ with $r^2 = 0.71$, where E_1 is the halfwave function of each phenolate.³⁵ Although their QSAR investigated the first one-electron reduction and our LFER examined the activation energy, the correlation of our LFER for 38 phenolates developed in this study has a comparable accuracy with $r^2 = 0.72$. For 1O_2 addition to phenols, the formation of a precursor complex is not the rate-determining step as we did not observe any correlation with $\Delta E^{\rm int}_{\rm ac}$ However, the formation of transition states strongly correlates with the observed rate constants, indicating that the functional groups on the benzene ring significantly affect the approach of $^{1}\mathrm{O}_{2}$ to the ring and addition to the π bond. For phenols and other compounds, the role of a functional group in the ¹O₂ addition to various ring structures will be discussed in detail in the next section.

Role of Functional Groups. The strong correlation observed in LFERs for the group of phenolates undergoing SET and all compounds undergoing $^{1}O_{2}$ addition indicates that the functional groups exert a profound role in changing the delocalization of the formal charge of the precursor complex. To further investigate the role of each functional group on the groups of phenolates and phenols, we compared the Hammett σ^{-} constants with the $\Delta G^{\rm act}_{\rm aq,SET}$ and $\Delta G^{\rm act}_{\rm aq,add}$ values, respectively. Hammett σ^{-} constants, which represent

the property of functional groups to accept electron density by through-resonance, were used to correlate with the half-wave function potentials.³⁹ Figure 2 shows the plots of the total of the σ^- constants vs the $\Delta G^{
m act}_{
m aq,SET}$ values for the group of phenolates and the $\Delta G^{\rm act}_{\rm aq,add}$ values for the group of phenols. Hammett constants are additive when a compound holds multiple-functional groups. The Hammett constant at the ortho position was assumed to be equal to the constant at the para position because of their similar resonance abilities.³⁵ Both plots show excellent correlations, indicating that the resonance ability of each functional group correlates with our $\Delta G^{\rm act}_{\rm ad}$ values for each reaction mechanism. It was apparent that the use of Hammett σ^- constants showed the best correlation among the use of other Hammett constants (e.g., σ) for both groups of phenolates and phenols, which was likely due to the significant difference in the Hammett constants for the strong electron-withdrawing functional groups (i.e., nitro). For example, using the σ constant (0.78 for ortho and para and 0.71 for meta position)¹⁰² for the nitro functional group(s) rather than the σ^- value $(1.27)^{102}$ resulted in an inconsistent overall trend for phenolates. The correlation between the Hammett σ^- constants and the $\Delta G^{
m act}_{
m aq,add}$ values for the group of phenolates (Figure S6 in the SI) was found to be inferior to the correlation with the $\Delta G^{\text{act}}_{\text{aq,SET}}$ values ($r^2 = 0.86$), which was likely due to not only the resonance effect of functional groups but also steric effects of the ¹O₂ addition to the benzene ring of phenolates. The reasonable correlation between the $k_{
m chem}$ values and $\Delta E^{
m int}_{
m aq}$ for the group of phenolates (Figure S3 in the SI) supports the involvement of the steric effect. For the

group of phenols undergoing the 1O2 addition, a similar correlation with the σ values ($r^2 = 0.84$) was observed (Figure S7 in the SI) due to an equivalent involvement of electrondonating/-withdrawing functionality to the resonance effect (see the Reaction Mechanisms section for the detailed discussion). Even though the development of the original Hammett constants was based on equilibrium constants, the general parameters of resonance ability indicate the strong quantitative relationship with the kinetic parameter (i.e., $\Delta G_{\text{ad}}^{\text{act}}$). Luo et al.⁵² did not observe any correlation between the Hammett constants and the theoretically calculated free energies of activation for the series of reactions between sulfate radical anion and aromatic compounds; however, they did not appear to include the outer-sphere solvent organization energies, which may have caused the inconsistent correlation. Our thorough consideration of the solvent organization procedure is included in Text S3 in the SI. We find that the accurate estimation of the outer-sphere solvent organization is key for estimating $\Delta G^{\rm act}_{\rm aq,SET}$ values, as was also investigated in the reactions of excited-state triplet sensitizers. 103

Reaction Mechanisms. For the group of phenolates, SET occurs on the dissociated OH functional group of a phenolate compound, and thus, the formation of a precursor complex plays a key role in the initial charge transfer. The SET is impacted by functional groups through resonance effects. In contrast, the ring structures that have C=C and/or C=N undergo electron transfer via resonance ring structures. The HOMO distributions of reactants (Table S5 in the SI) support the possible reactive sites proposed above. Electron transfer between the dissociated OH functional group and ¹O₂ requires much less energy than the transfer between the benzene ring and 1O2, resulting in a steeper slope for the group of phenolates (Figure 1). While the SET reactions of the majority of phenolates are exergonic (i.e., $\Delta G^{\text{react}}_{\text{aq,SET}} < 0$), reactions with strong electron-withdrawing groups (i.e., nitro, cyano, trichloro) are endergonic (i.e., $\Delta G^{\text{react}}_{\text{aq,SET}} > 0$). The k_{chem} values for these compounds are $10^5 - 10^7 \text{ M}^{-1} \text{ s}^{-1}$, indicating the significant contribution of a backward reaction or overrun of the kinetics.

When phenolates undergo ¹O₂ addition, the negative charge of the dissociated OH functional group is delocalized on the benzene ring through the resonance structures (Figure S8 in the SI), which favors ¹O₂ addition at the ortho and para positions. 104 The transition states identified in this study confirmed the unfavorable addition of ¹O₂ on phenolates at the meta position. This is also supported by $\Delta G^{\text{react}}_{\text{aq,add}}$ values of -14.2 kcal/mol for the meta positions compared to significantly exergonic values of -51.9 and -53.4 kcal/mol at the ortho and para positions, respectively. Electron-donating functional groups at the ortho and para positions generate a repulsive force between the delocalized negative ions and free electrons of the donating functional groups, which makes the functional groups unstable and inhibits the addition of ¹O₂ to those sites. In contrast, the presence of electron-withdrawing functional groups at the ortho and para positions withdraws the delocalized negative ions and stabilizes the resonance structures, which promotes the stepwise addition of ¹O₂ to

It is well known that the hydroxyl group of phenol donates electron density to ortho and para positions, and the para carbon atom that is more susceptible to $^1{\rm O}_2$ enhances 1,4-cycloaddition more so than the ortho carbon atom. 21 Our observations of the $\Delta G^{\rm act}_{\rm aq,add}$ values for the reaction with

ı

phenol at the 1,4-, 2,5-, and 3,6-positions confirm this (see Table S4 in the SI), and all additions followed the concerted mechanism. The $\Delta G^{\rm act}_{\rm aq,add}$ values resulting from the 1,4addition are less than those resulting from 2,5- and 3,6additions by 2-9 kcal/mol. When ${}^{1}O_{2}$ approaches those positions, a partial positive charge develops on the phenol and a partial negative charge develops on ¹O₂. When electrondonating groups are present at the para position, the partial positive charge is stabilized resulting in lower $\Delta G^{\rm act}_{\rm aq,add}$ values. Electron-withdrawing groups at the same position develop partial positive charges, which does not stabilize the charge and increase the $\Delta G^{
m act}_{
m aq,add}$ values. The electron-donating/withdrawing properties of functional groups of phenols play a more substantial role in the position of ¹O₂ addition than those of phenolates. The reaction product of the para-ipso intermediate that results from the 1,4-addition forms para-benzoquinone via a unimolecular isomerization followed by a facile mechanism.²¹

The furan derivatives (nos. 70–72) show preferable $^1{\rm O}_2$ addition to carbon atoms of a five-membered ring at the 1,4-positions. The presence of a single or multiple electron-donating functional group(s) (i.e., methyl and hydroxymethyl) at the 1- and/or 4-positions increases the electron density for carbon atoms at the 1- and/or 4-positions or σ -occupancy of in-ring atomic orbitals. 105 A temperature-dependent, time-resolved phosphorescence measurement determined the experimental $\Delta G^{\rm act}_{\rm aq,add}$ for furfuryl alcohol to be 6.5 \pm 0.12 kcal/mol, 90 which is close to our value of 3.5 kcal/mol. The $\Delta G^{\rm act}_{\rm aq,SET}$ value of 19.8 kcal/mol supports a preferable $^1{\rm O}_2$ addition to furfuryl alcohol. Diels—Alder, oxygen-bridged adducts are formed following ring cleavage and production of ketones and aldehydes. 106

Three aromatic amines investigated in this study exhibit different reaction mechanisms due to their unique structures. While 2-dimethylamino-5,6-dimethylpyrimidin-4-ol (no. 75) undergoes ${}^{1}O_{2}$ addition, N,N-dimethyl-4-nitroaniline (no. 73) and $N_1N_2N_3N_4$ -tetramethyl-p-phenylenediamine (TMPD) (no. 74) undergo SET (10.5 and 1.3 kcal/mol of the $\Delta G_{\text{aq,SET}}^{\text{act}}$ value, respectively), which is in agreement with the experimental observation that confirmed the formation of TMPD+•.107 TMPD is known as a charge-transfer quencher resulting from an ¹O₂-aniline exciplex. ¹⁰⁸ This dominant SET mechanism for TMPD was used to validate our Marcus calculations (Text S3). Due to the dominant SET mechanism, the data points for these two compounds do not adhere to the LFER of ¹O₂ addition (Figure 1) and were not included in the correlation analysis. The addition of ¹O₂ to the C=C double bond of a pyrimidine ring at the 1,4-positions of 2dimethylamino-5,6-dimethylpyrimidin-4-ol is supported by the experimental observation and is consistent with our $\Delta G^{\rm act}_{\rm aq,add}$ value of 6.0 kcal/mol. Dialkyl sulfides such as diethyl sulfide (no. 77) do not have

Dialkyl sulfides such as diethyl sulfide (no. 77) do not have an appropriate low-lying excited state to deactivate $^1\mathrm{O}_2$ by an electronic energy-transfer mechanism for physical quenching that produces ground-state oxygen as a product. ¹¹⁰ Instead, the $^1\mathrm{O}_2$ addition to the sulfur functional group occurs as a donation of the sulfur lone pair into the empty $\pi_{\rm g}$ orbital of $^1\mathrm{O}_2$ to form persulfoxide. We obtained very similar $\Delta G^{\rm act}_{\rm aq,add}$ values (5–6 kcal/mol) for all sulfide compounds in the aqueous phase. The gas-phase reactions of $^1\mathrm{O}_2$ with sulfide require little free energy of activation or a negative value. ¹¹¹ In the aqueous phase, polar water molecules stabilize the transition state more effectively than organic solvents like

Scheme 2. Major Reaction Mechanisms of ¹O₂ with Structurally Diverse Organic Compounds

benzene (7 kcal/mol) and acetone (13 kcal/mol),²⁹ which is consistent with our $\Delta G^{\text{act}}_{\text{aq,add}}$ values.

Imidazole (no. 84) and the derivatives (nos. 80–83) are known to react with $^{1}O_{2}$ through a Diels–Alder process (1,4-addition), which was confirmed by investigating all of the possible elementary reaction pathways (Text S7, Figure S9, and Table S6 in the SI). We determined 5.9 kcal/mol for the $\Delta G^{\rm act}_{\rm aq,add}$ value for histidine, which is in good agreement with the 8.7 kcal/mol reported by the high-level CCSD(T) method with a COSMO solvation model. 112

While previous experimental studies postulate that the $^{1}O_{2}$ reacts with the thiourea functional group or sulfur atom, 113 the detailed mechanisms have not been elucidated yet. The free energy of reaction was slightly exergonic, -8.0 kcal/mol of the $\Delta G^{\rm react}_{\rm aq,add}$ value, suggesting that this is thermodynamically favorable. The $\Delta G^{\rm act}_{\rm aq,add}$ for the same reaction was 6.0 kcal/mol. The $\Delta G^{\rm react}_{\rm aq,add}$ values for the thiourea derivatives (nos. 86 and 87) were -7.2 and -8.0 kcal/mol, respectively, and the $\Delta G^{\rm act}_{\rm aq,add}$ values were 6.3 and 6.3 kcal/mol, respectively. We propose that the mechanism of $^{1}O_{2}$ with thioureas be the enereaction. The detailed discussion on thiourea can be found in Text S7 and Figure S10 in the SI.

Pyrrole (no. 88) and the derivatives (nos. 89 and 90) undergo two possible pathways, (1) 1,2-cycloaddition to form a dioxetane intermediate 114 or (2) 1,4-cycloaddition to form an endoperoxide intermediate. We obtained 2.0 and 6.9 kcal/mol of the $\Delta G^{\rm act}_{\rm aq,add}$ values for the 1,4-cycloaddition and the 1,2-cycloaddition, respectively, confirming the dominant 1,4-addition. The phenyl group of 3-phenylpyrrole (no. 90) donates electrons 116 and enhances the 1,4-cycloaddition of $^{1}{\rm O}_{2}$, reducing the value to 1.8 kcal/mol. The cyano functional group at the same 3-position withdraws electrons and significantly increases the $\Delta G^{\rm act}_{\rm aq,add}$ value to 7.2 kcal/mol for the same reaction mechanism. The SET reaction for pyrrole

requires significantly more energy and is thermodynamically unfavorable.

The three aliphatic amines investigated in this study include 2,2,6,6-tetramethylpiperidin-4-ol (no. 91), 1,4-diazabicyclo-[2,2,2]octane (no. 92), and alanine (no. 93). Our $\Delta G_{\text{ad,SET}}^{\text{act}}$ values for the compounds are consistent with the trend of the $k_{\rm chem}$ values, which suggests that SET is the dominant mechanism for these sterically hindered amine compounds, as postulated by several experimental studies. 117 The largest $k_{
m chem}$ value (i.e., smallest $\Delta G^{
m act}_{
m aq,SET}$ value) was predicted for 1,4-diazabicyclo [2,2,2]octane, (DABCO). The aliphatic amine species has two tertiary amines that can be accessed externally by ¹O₂, which promotes the initial charge separation. 2,2,6,6-Tetramethyl-4-piperidinol also has a tertiary amine that is sterically hindered by four methyl functional groups that ¹O₂ cannot access for charge separation. Only alanine, a primary amine, exhibited potential SET and ¹O₂ addition mechanisms due to accessibility of ¹O₂ to the amine.

Indole (no. 99) and the derivatives (nos. 94–98) are a group of aromatic heterocyclic compounds that contain both a five-membered pyrrole and a six-membered benzene ring. Due to the benzene ring, 1,4-addition to the five-membered pyrrole of indole requires larger $\Delta G^{\rm act}_{\rm aq,add}$ energies than those for pyrrole by 4.8 kcal/mol, which is consistent with the $k_{\rm chem}$ values obtained by experiments. We fully investigated stepwise and concerted addition to the pyrrole and benzene rings and found the lowest-energy transition-state structure for the LFER for 1,4-addition to the pyrrole ring of indole (Text S7, Figure S11, and Table S7 in the SI). 119,120

Scheme 2 summarizes the major $^{1}O_{2}$ reaction mechanisms of structurally diverse organic compounds investigated in this study.

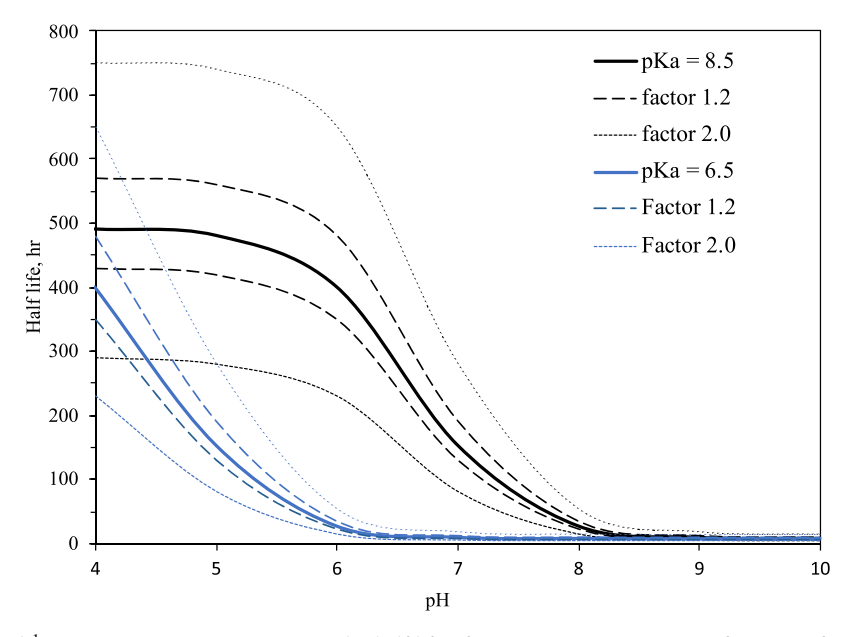


Figure 3. Impact of pK_a and 1O_2 rate constant estimation on the half-life of a target contaminant as a function of pH.

■ ENVIRONMENTAL IMPLICATION

This study highlights the elementary reaction pathways and kinetics induced by the reaction of 1O2 with a variety of organic compounds. The LFERs developed in this study can predict the k_{chem} values within a factor of 1.2 of the experimental values. As a practical application, we developed a non-steady-state kinetic model and estimated the half-lives of two compounds as a function of pH. One compound has a p K_a = 8.5 and the other compound has a p K_a = 6.5, with k_{chem} = 10⁸ and 10⁶ M⁻¹ s⁻¹ for the dissociated and nondissociated forms, respectively. The detailed kinetic model description is presented in Text S8 in the SI. Figure 3 demonstrates that there are larger impacts of k_{chem} values on the half-lives at lower pH. Differences of a factor of 1.2 and 2.0 in the experimental $k_{\rm chem}$ values result in differences of greater than 60 and 200 h in the half-lives, respectively, at pH = 4. The impact is lessened near-neutral pH and above the pK_a values because the dissociated form is more dominant and significantly enhances the overall degradation rates. At pH = 10, differences of a factor 1.2 and 2.0 result in up to 1.2 and 6 h of differences in the half-lives, respectively. The LFERs, which are accurate within a factor of 1.2, would result in up to 17 h of difference in the estimated half-life of a compound with a p K_a of 8.5 at neutral pH. The impact is significantly reduced for compounds with a p K_a of 6.5 due to a more rapid reaction of ${}^{1}O_2$ with the dissociated form.

ASSOCIATED CONTENT

Supporting Information

The Supporting Information is available free of charge at https://pubs.acs.org/doi/10.1021/acs.est.1c01712.

Additional information for 11 figures: a whisker plot, IRC plots, $\ln k_{\rm chem}$ vs $\Delta E^{\rm int}_{\rm aq}$, Rehm—Weller plot, $\ln k_{\rm chem}$ vs total charge, Hammett plots; eight tables: method validation, the $\Delta G^{\rm act}_{\rm add}$ values, HOMO, and elementary reactions; and sight tables, seven texts (PDF)

z-matrix of all transition states and IRC results (PDF)

AUTHOR INFORMATION

Corresponding Author

Daisuke Minakata — Department of Civil and Environmental Engineering, Michigan Technological University, Houghton, Michigan 49931, United States; orcid.org/0000-0003-3055-3880; Phone: +1-906-487-1830; Email: dminakat@mtu.edu; Fax: +1-906-487-2943

Authors

Benjamin Barrios — Department of Civil and Environmental Engineering, Michigan Technological University, Houghton, Michigan 49931, United States

Benjamin Mohrhardt – Department of Civil and Environmental Engineering, Michigan Technological University, Houghton, Michigan 49931, United States

Paul V. Doskey — College of Forest Resources and Environmental Science, Michigan Technological University, Houghton, Michigan 49931, United States

Complete contact information is available at: https://pubs.acs.org/10.1021/acs.est.1c01712

Notes

The authors declare no competing financial interest.

ACKNOWLEDGMENTS

This work was supported by the National Science Foundation Award CHE-1808052. Any opinions, findings, conclusions, or recommendations expressed in this publication are those of the authors and do not necessarily reflect the view of the supporting organization. D.M. appreciates helpful comments given by Dr. Silvio Canonica from Eawag. The authors appreciate the support for the use of Michigan Tech HPC cluster "Superior".

REFERENCES

- (1) Zepp, R. G.; Wolfe, N. L.; Baughman, G. L.; Hollis, R. C. Singlet oxygen in natural waters. *Nature* 1977, 267, 421–423.
- (2) Lee, J.; von Gunten, U.; Kim, J.-H. Persulfate-Based Advanced Oxidation: Critical Assessment of Opportunities and Roadblocks. *Environ. Sci. Technol.* **2020**, *54*, 3064–3081.

- (3) Matsuura, T. Bio-mimetic oxygenation. *Tetrahedron* 1977, 33, 2869–2905.
- (4) Zhang, Z.; He, X.; Zhou, C.; Reaume, M.; Wu, M.; Liu, B.; Lee, B. P. Iron Magnetic Nanoparticle-Induced ROS Generation from Catechol-Containing Microgel for Environmental and Biomedical Applications. ACS Appl. Mater. Interfaces 2020, 12, 21210–21220.
- (5) Frimer, A. A. Oxidative Processes in Biological Systems and Their Role in Plant Senescence. In *Developments in Crop Science*; Leshem, Y. A. Y.; Halevy, A. H.; Frenkel, C., Eds.; Elsevier: 1986; Chapter 5, Vol. 8, pp 84–99.
- (6) Wasserman, H. H.; Ives, J. L. Singlet oxygen in organic synthesis. *Tetrahedron* **1981**, *37*, 1825–1852.
- (7) Bregnhøj, M.; Westberg, M.; Jensen, F.; Ogilby, P. R. Solvent-dependent singlet oxygen lifetimes: temperature effects implicate tunneling and charge-transfer interactions. *Phys. Chem. Chem. Phys.* **2016**, *18*, 22946–22961.
- (8) Merkel, P. B.; Kearns, D. R. Remarkable solvent effects on the lifetime of $^{1}\Delta_{o}$ oxygen. *J. Am. Chem. Soc.* **1972**, *94*, 1029–1030.
- (9) Larson, R. A.; Weber, E. J. Reaction Mechanisms in Environmental Organic Chemistry, 1st ed.; CRC Press, 1994; p 368.
- (10) Larson, R. A.; Marley, K. A. In *Handbook of Environmental Chemistry*; Boule, P., Ed.; Springer-Verlag: Berlin Heidelberg GmbH, 1999; Vol. 2, Part F, pp 123–137.
- (11) Hoigné, J.; Faust, B. C.; Haag, W. R.; Scully, F. E.; Zepp, R. G. Aquatic Humic Substances as Sources and Sinks of Photochemically Produced Transient Reactants. *Aquatic Humic Substances*; American Chemical Society, 1988; Vol. 219, pp 363–381.
- (12) Schwarzenbach, R. P.; Gschwend, P. M.; Imboden, D. M. Environmental Organic Chemistry; John Wiley & Sons, Inc., 2002.
- (13) Lee, J.; Mackeyev, Y.; Cho, M.; Li, D.; Kim, J.-H.; Wilson, L. J.; Alvarez, P. J. J. Photochemical and Antimicrobial Properties of Novel C60 Derivatives in Aqueous Systems. *Environ. Sci. Technol.* **2009**, 43, 6604–6610.
- (14) Manjón, F.; Villén, L.; García-Fresnadillo, D.; Orellana, G. On the Factors Influencing the Performance of Solar Reactors for Water Disinfection with Photosensitized Singlet Oxygen. *Environ. Sci. Technol.* **2008**, *42*, 301–307.
- (15) Pitts, J. N.; Khan, A. U.; Smith, E. B.; Wayne, R. P. Singlet oxygen in the environmental sciences. Singlet molecular oxygen and photochemical air pollution. *Environ. Sci. Technol.* **1969**, *3*, 241–247.
- (16) Nathan, C.; Ding, A. SnapShot: Reactive Oxygen Intermediates (ROI). Cell 2010, 140, 951.e2.
- (17) Clennan, E. L.; Pace, A. Advances in singlet oxygen chemistry. *Tetrahedron* **2005**, *61*, 6665–6691.
- (18) Frimer, A. A. The reaction of singlet oxygen with olefins: the question of mechanism. *Chem. Rev.* **1979**, *79*, 359–387.
- (19) Saito, I.; Matsuura, T.; Inoue, K. Formation of superoxide ion from singlet oxygen. Use of a water-soluble singlet oxygen source. *J. Am. Chem. Soc.* **1981**, *103*, 188–190.
- (20) Thomas, M. J.; Foote, C. S. Chemistry Of Singlet Oxygen—XXVI. Photogeneration OF Phenols. *Photochem. Photobiol.* **1978**, 27, 683–693.
- (21) Al-Nu'airat, J.; Dlugogorski, B. Z.; Gao, X.; Zeinali, N.; Skut, J.; Westmoreland, P. R.; Oluwoye, I.; Altarawneh, M. Reaction of phenol with singlet oxygen. *Phys. Chem. Chem. Phys.* **2019**, *21*, 171–183.
- (22) Armstrong, D. A.; Huie, R. E.; Koppenol, W. H.; Lymar, S. V.; Merényi, G.; Neta, P.; Ruscic, B.; Stanbury, D. M.; Steenken, S.; Wardman, P. Standard electrode potentials involving radicals in aqueous solution: inorganic radicals (IUPAC Technical Report). *Pure Appl. Chem.* **2015**, *87*, 1139–1150.
- (23) Stephenson, L. M.; Grdina, M. J.; Orfanopoulos, M. Mechanism of the ene reaction between singlet oxygen and olefins. *Acc. Chem. Res.* **1980**, *13*, 419–425.
- (24) Singleton, D. A.; Hang, C.; Szymanski, M. J.; Meyer, M. P.; Leach, A. G.; Kuwata, K. T.; Chen, J. S.; Greer, A.; Foote, C. S.; Houk, K. N. Mechanism of Ene Reactions of Singlet Oxygen. A Two-Step No-Intermediate Mechanism. *J. Am. Chem. Soc.* **2003**, *125*, 1319–1328.

- (25) Rehm, D.; Weller, A. Kinetics of Fluorescence Quenching by Electron and H-Atom Transfer. *Isr. J. Chem.* **1970**, *8*, 259–271.
- (26) Yuan, C.; Chakraborty, M.; Canonica, S.; Weavers, L. K.; Hadad, C. M.; Chin, Y.-P. Isoproturon Reappearance after Photosensitized Degradation in the Presence of Triplet Ketones or Fulvic Acids. *Environ. Sci. Technol.* **2016**, *50*, 12250–12257.
- (27) Wilkinson, F.; Helman, W. P.; Ross, A. B. Rate Constants for the Decay and Reactions of the Lowest Electronically Excited Singlet State of Molecular Oxygen in Solution. An Expanded and Revised Compilation. *J. Phys. Chem. Ref. Data* 1995, 24, 663.
- (28) Scully, F. E.; Hoigné, J. Rate constants for reactions of singlet oxygen with phenols and other compounds in water. *Chemosphere* 1987, 16, 681–694.
- (29) Jensen, F.; Greer, A.; Clennan, E. L. Reaction of Organic Sulfides with Singlet Oxygen. A Revised Mechanism. *J. Am. Chem. Soc.* **1998**, 120, 4439–4449.
- (30) Lacombe, S.; Cardy, H.; Simon, M.; Khoukh, A.; Soumillion, J. P.; Ayadim, M. Oxidation of sulfides and disulfides under electron transfer or singlet oxygen photosensitization using soluble or grafted sensitizers. *Photochem. Photobiol. Sci.* **2002**, *1*, 347–354.
- (31) Saito, I.; Matsuura, T. In Singlet Oxygen; Wasserman, H. H.; Murray, R. W., Eds.; Academic: New York, 1979; pp 511-574.
- (32) Nonell, S.; Flors, C. Singlet Oxygen: Applications in Biosciences and Nanosciences; Royal Society of Chemistry: Cambridge, U.K., 2016; Vol. 1.
- (33) Canonica, S.; Tratnyek, P. G. Quantitative structure-activity relationships for oxidation reactions of organic chemicals in water. *Environ. Toxicol. Chem.* **2003**, *22*, 1743–1754.
- (34) Suatoni, J. C.; Snyder, R. E.; Clark, R. O. Voltammetric studies of phenol and aniline ring substitution. *Anal. Chem.* **1961**, *33*, 1894–1897.
- (35) Arnold, W. A.; Oueis, Y.; O'Connor, M.; Rinaman, J. E.; Taggart, M. G.; McCarthy, R. E.; Foster, K. A.; Latch, D. E. QSARs for phenols and phenolates: oxidation potential as a predictor of reaction rate constants with photochemically produced oxidants. *Environ. Sci.: Processes Impacts* **2017**, *19*, 324–338.
- (36) Nolte, T. M.; Peijnenburg, W. J. G. M. Aqueous-phase photooxygenation of enes, amines, sulfides and polycyclic aromatics by singlet $(^{1}\Delta_{\rm g})$ oxygen: prediction of rate constants using orbital energies, substituent factors and quantitative structure–property relationships. *Environ. Chem.* **2017**, *14*, 442–450.
- (37) Rorije, E.; Peijnenburg, W. J. G. M. QSARs for oxidation of phenols in the aqueous environment, suitable for risk assessment. *J. Chemom.* **1996**, *10*, 79–93.
- (38) Zhu, C. M.; Wang, L. Y.; Kong, L. R.; Yang, X.; Wang, L. S.; Zheng, S. J.; Chen, F. L.; Feng, M. Z.; Huang, Z. QSPR study of quenching of singlet oxygen by aliphatic amines. *Toxicol. Environ. Chem.* **2001**, *79*, 47–54.
- (39) Tratnyek, P. G.; Hoigne, J. Oxidation of substituted phenols in the environment: a QSAR analysis of rate constants for reaction with singlet oxygen. *Environ. Sci. Technol.* **1991**, *25*, 1596–1604.
- (40) Kohn, W.; Sham, L. J. Self-Consistent Equations Including Exchange and Correlation Effects. *Phys. Rev.* **1965**, *140*, A1133–A1138.
- (41) Cramer, C. J. Essentials of Computational Chemistry: Theories and Models, 2nd ed.; Wiley, 2004.
- (42) Cramer, C. J.; Truhlar, D. G. Implicit Solvation Models: Equilibria, Structure, Spectra, and Dynamics. *Chem. Rev.* **1999**, *99*, 2161–2200.
- (43) Trogolo, D.; Mishra, B. K.; Heeb, M. B.; von Gunten, U.; Arey, J. S. Molecular Mechanism of NDMA Formation from N,N-Dimethylsulfamide During Ozonation: Quantum Chemical Insights into a Bromide-Catalyzed Pathway. *Environ. Sci. Technol.* **2015**, 49, 4163–4175.
- (44) Kamath, D.; Mezyk, S. P.; Minakata, D. Elucidating the Elementary Reaction Pathways and Kinetics of Hydroxyl Radical-Induced Acetone Degradation in Aqueous Phase Advanced Oxidation Processes. *Environ. Sci. Technol.* **2018**, *52*, *7763*–7774.

- (45) Kamath, D.; Minakata, D. Emerging investigators series: ultraviolet and free chlorine aqueous-phase advanced oxidation process: kinetic simulations and experimental validation. *Environ. Sci. Water Res. Technol.* **2018**, 4, 1231–1238.
- (46) Eyring, H.; Gershinowitz, H.; Sun, C. E. The Absolute Rate of Homogeneous Atomic Reactions. *J. Chem. Phys.* **1935**, *3*, 786–796.
- (47) Minakata, D.; Kamath, D.; Maetzold, S. Mechanistic Insight into the Reactivity of Chlorine-Derived Radicals in the Aqueous-Phase UV-Chlorine Advanced Oxidation Process: Quantum Mechanical Calculations. *Environ. Sci. Technol.* **2017**, *51*, 6918–6926.
- (48) Minakata, D.; Song, W.; Mezyk, S. P.; Cooper, W. J. Experimental and theoretical studies on aqueous-phase reactivity of hydroxyl radicals with multiple carboxylated and hydroxylated benzene compounds. *Phys. Chem. Chem. Phys.* **2015**, *17*, 11796–11812.
- (49) Minakata, D.; Mezyk, S. P.; Jones, J. W.; Daws, B. R.; Crittenden, J. C. Development of Linear Free Energy Relationships for Aqueous Phase Radical-Involved Chemical Reactions. *Environ. Sci. Technol.* **2014**, *48*, 13925–13932.
- (50) Minakata, D.; Song, W.; Crittenden, J. Reactivity of Aqueous Phase Hydroxyl Radical with Halogenated Carboxylate Anions: Experimental and Theoretical Studies. *Environ. Sci. Technol.* **2011**, 45, 6057–6065.
- (51) Minakata, D.; Crittenden, J. Linear Free Energy Relationships between Aqueous phase Hydroxyl Radical Reaction Rate Constants and Free Energy of Activation. *Environ. Sci. Technol.* **2011**, *45*, 3479—3486.
- (52) Luo, S.; Wei, Z.; Dionysiou, D. D.; Spinney, R.; Hu, W.-P.; Chai, L.; Yang, Z.; Ye, T.; Xiao, R. Mechanistic insight into reactivity of sulfate radical with aromatic contaminants through single-electron transfer pathway. *Chem. Eng. J.* **2017**, 327, 1056–1065.
- (53) Tentscher, P. R.; Lee, M.; von Gunten, U. Micropollutant Oxidation Studied by Quantum Chemical Computations: Methodology and Applications to Thermodynamics, Kinetics, and Reaction Mechanisms. *Acc. Chem. Res.* **2019**, *52*, 605–614.
- (54) Smoluchowski, M. v. Versuch einer mathematischen Theorie der Koagulationskinetik kolloider Lösungen. Z. Phys. Chem. 1918, 92U, 129–168.
- (55) Collins, F. C.; Kimball, G. E. Diffusion-controlled reaction rates. *J. Colloid Sci.* **1949**, *4*, 425–437.
- (56) Wavefunction, I. Spartan'18; Wavefunction, Inc.: Irvine, California, 2018.
- (57) Halgren, T. A.; Nachbar, R. B. Merck molecular force field. IV. conformational energies and geometries for MMFF94. *J. Comput. Chem.* **1996**, *17*, 587–615.
- (58) Rosokha, S. V.; Kochi, J. K. Fresh Look at Electron-Transfer Mechanisms via the Donor/Acceptor Bindings in the Critical Encounter Complex. *Acc. Chem. Res.* **2008**, *41*, 641–653.
- (59) Marcus, R. A. Chemical and Electrochemical Electron-Transfer Theory. *Annu. Rev. Phys. Chem.* **1964**, *15*, 155–196.
- (60) Marcus, R. A. Electron transfer reactions in chemistry theory and experiment. *J. Electroanal. Chem.* **1997**, 438, 251–259.
- (61) Zhao, Y.; Truhlar, D. G. The M06 suite of density functionals for main group thermochemistry, thermochemical kinetics, non-covalent interactions, excited states, and transition elements: two new functionals and systematic testing of four M06-class functionals and 12 other functionals. *Theor. Chem. Acc.* 2008, 120, 215–241.
- (62) Marenich, A. V.; Cramer, C. J.; Truhlar, D. G. Universal Solvation Model Based on Solute Electron Density and on a Continuum Model of the Solvent Defined by the Bulk Dielectric Constant and Atomic Surface Tensions. *J. Phys. Chem. B* **2009**, *113*, 6378–6396.
- (63) Gräfenstein, J.; Kraka, E.; Filatov, M.; Cremer, D. Can Unrestricted Density-Functional Theory Describe Open Shell Singlet Biradicals? *Int. J. Mol. Sci.* **2002**, *3*, 360–394.
- (64) Saito, T.; Nishihara, S.; Kataoka, Y.; Nakanishi, Y.; Matsui, T.; Kitagawa, Y.; Kawakami, T.; Okumura, M.; Yamaguchi, K. Transition state optimization based on approximate spin-projection (AP) method. *Chem. Phys. Lett.* **2009**, *483*, 168–171.

- (65) Saito, T.; Nishihara, S.; Kataoka, Y.; Nakanishi, Y.; Kitagawa, Y.; Kawakami, T.; Yamanaka, S.; Okumura, M.; Yamaguchi, K. Reinvestigation of the Reaction of Ethylene and Singlet Oxygen by the Approximate Spin Projection Method. Comparison with Multi-reference Coupled-Cluster Calculations. *J. Phys. Chem. A* **2010**, *114*, 7967–7974.
- (66) Boys, S. F.; Bernardi, F. The calculation of small molecular interactions by the differences of separate total energies. Some procedures with reduced errors. *Mol. Phys.* **1970**, *19*, 553–566.
- (67) Ardura, D.; López, R.; Sordo, T. L. Relative Gibbs Energies in Solution through Continuum Models: Effect of the Loss of Translational Degrees of Freedom in Bimolecular Reactions on Gibbs Energy Barriers. J. Phys. Chem. B 2005, 109, 23618–23623.
- (68) Pu, J.; Gao, J.; Truhlar, D. G. Multidimensional Tunneling, Recrossing, and the Transmission Coefficient for Enzymatic Reactions. *Chem. Rev.* **2006**, *106*, 3140–3169.
- (69) Frisch, M. J.; Trucks, G. W.; Schlegel, H. B.; Scuseria, G. E.; Robb, M. A.; Cheeseman, J. R.; Scalmani, G.; Barone, V.; Petersson, G. A.; Nakatsuji, H.; Li, X.; Caricato, M.; Marenich, A. V.; Bloino, J.; Janesko, B. G.; Gomperts, R.; Mennucci, B.; Hratchian, H. P.; Ortiz, J. V.; Izmaylov, A. F.; Sonnenberg, J. L.; Williams; Ding, F.; Lipparini, F.; Egidi, F.; Goings, J.; Peng, B.; Petrone, A.; Henderson, T.; Ranasinghe, D.; Zakrzewski, V. G.; Gao, J.; Rega, N.; Zheng, G.; Liang, W.; Hada, M.; Ehara, M.; Toyota, K.; Fukuda, R.; Hasegawa, J.; Ishida, M.; Nakajima, T.; Honda, Y.; Kitao, O.; Nakai, H.; Vreven, T.; Throssell, K.; Montgomery, J. A., Jr.; Peralta, J. E.; Ogliaro, F.; Bearpark, M. J.; Heyd, J. J.; Brothers, E. N.; Kudin, K. N.; Staroverov, V. N.; Keith, T. A.; Kobayashi, R.; Normand, J.; Raghavachari, K.; Rendell, A. P.; Burant, J. C.; Iyengar, S. S.; Tomasi, J.; Cossi, M.; Millam, J. M.; Klene, M.; Adamo, C.; Cammi, R.; Ochterski, J. W.; Martin, R. L.; Morokuma, K.; Farkas, O.; Foresman, J. B.; Fox, D. J. Gaussian 16, revision C.01; Gaussian, Inc.: Wallingford, CT, 2016.
- (70) Werner, H.-J.; Knowles, P. J.; Knizia, G.; Manby, F. R.; Schütz, M. Molpro: a general-purpose quantum chemistry program package. *Wiley Interdiscip. Rev.: Comput. Mol. Sci.* **2012**, *2*, 242–253.
- (71) Brezonik, P. L. Chemical Kinetics and Process Dynamics in Aquatic Systems, 1st ed.; CRC Press, 1993.
- (72) Matouschek, A.; Kellis, J. T.; Serrano, L.; Fersht, A. R. Mapping the transition state and pathway of protein folding by protein engineering. *Nature* **1989**, 340, 122–126.
- (73) Marcus, R. A. Theoretical relations among rate constants, barriers, and Broensted slopes of chemical reactions. *J. Phys. Chem. A* **1968**, 72, 891–899.
- (74) Greig, I. R. The analysis of enzymic free energy relationships using kinetic and computational models. *Chem. Soc. Rev.* **2010**, 39, 2272–2301.
- (75) Klähn, M.; Rosta, E.; Warshel, A. On the mechanism of hydrolysis of phosphate monoesters dianions in solutions and proteins. *J. Am. Chem. Soc.* **2006**, *128*, 15310–15323.
- (76) Palumbo, M. C.; García, N. A.; Argüello, G. A. The interaction of singlet molecular oxygen $O_2(^1\Delta_g)$ with indolic derivatives. Distinction between physical and reactive quenching. *J. Photochem. Photobiol., B* **1990**, *7*, 33–42.
- (77) Luiz, M.; Gutiérrez, M. I.; Bocco, G.; García, N. A. Solvent effect on the reactivity of monosubstituted phenols towards singlet molecular oxygen $(O_2(^1\Delta_g))$ in alkaline media. *Can. J. Chem.* **1993**, 71, 1247–1252.
- (78) Kruk, I.; Lichszteld, K.; Michalska, T.; Paraskevas, S. M. The influence of some biological antioxidants on the light emission from the oxytetracycline oxidation reaction. *Toxicol. Environ. Chem.* **1992**, 35, 167–173.
- (79) Bocco, G.; Luiz, M.; Gutiérrez, M. I.; Garcia, N. A. Influence of the nuclear substitution on the sensitized photooxidation of model compounds for phenolic-type pesticides. *J. Prakt. Chem.* **1994**, *336*, 243–246.
- (80) Sur, B.; De Laurentiis, E.; Minella, M.; Maurino, V.; Minero, C.; Vione, D. Photochemical transformation of anionic 2-nitro-4-chlorophenol in surface waters: Laboratory and model assessment of

- the degradation kinetics, and comparison with field data. *Sci. Total Environ.* **2012**, 426, 296–303.
- (81) Bertolotti, S. G.; García, N. A.; Argüello, G. A. Effect of the peptide bond on the singlet-molecular-oxygen-mediated sensitized photo-oxidation of tyrosine and tryptophan dipeptides. A kinetic study. *J. Photochem. Photobiol., B* **1991**, *10*, 57–70.
- (82) Miskosky, S.; Bertolotti, S. G.; García, N. A.; Argüello, G. A. On the $O_2(^1\Delta_g)$ -mediated photooxidative behaviour of tripeptide glycyltyrosyl-alanine in alkaline medium. A kinetic study. *Amino Acids* **1993**, 4, 101–110.
- (83) Seely, G. R. Mechanisms of the photosensitized oxidation of tyramine. *Photochem. Photobiol.* **1977**, 26, 115–123.
- (84) Mártire, D. O.; Evans, C.; Bertolotti, S. G.; Braslavsky, S. E.; García, N. A. Singlet molecular oxygen $[O_2(^1\Delta_g)]$ production and quenching by hydroxybiphenyls. *Chemosphere* **1993**, *26*, 1691–1701.
- (85) Okamoto, K.-I.; Hondo, F.; Itaya, A.; Kusabayashi, S. Kinetics of dye-sensitized photo-degradation of aqueous phenol. *J. Chem. Eng. Ipn.* **1982**, *15*, 368–375.
- (86) de Mol, N. J.; van Henegouwen, G. M. J. B. Formation of singlet molecular oxygen by 8-methoxypsoralen*. *Photochem. Photobiol.* **1979**, *30*, *331*–*335*.
- (87) Barboy, N.; Krajlj, I. On the reactivity of singlet oxygen in aqueous micellar systems. *J. Photochem.* **1978**, *9*, 336–337.
- (88) Manring, L. E.; Foote, C. S. Chemistry of singlet oxygen. 37. One-electron oxidation of tetramethylphenylenediamine by singlet oxygen. *J. Phys. Chem. B* **1982**, *86*, 1257–1259.
- (89) Usui, Y.; Tsukada, M.; Nakamura, H. Kinetic studies of photosensitized oxygenation by singlet oxygen in aqueous micellar solutions. *Bull. Chem. Soc. Jpn.* **1978**, *51*, 379–384.
- (90) Appiani, E.; Ossola, R.; Latch, D. E.; Erickson, P. R.; McNeill, K. Aqueous singlet oxygen reaction kinetics of furfuryl alcohol: effect of temperature, pH, and salt content. *Environ. Sci.: Processes Impacts* **2017**, *19*, 507–516.
- (91) Gottfried, V.; Kimel, S. Temperature effects on photosensitized processes. *J. Photochem. Photobiol., B* **1991**, *8*, 419–430.
- (92) Gottfried, V.; Peled, D.; Winkelman, J. W.; Kimel, S. Photosensitizers in organized media: singlet oxygen production and spectral properties. *Photochem. Photobiol.* **1988**, 48, 157–163.
- (93) Dixon, S. R.; Wells, C. H. J. Dye-sensitised photo-oxidation of 2-dimethylamino-5,6- dimethylpyrimidin-4-ol in aqueous solution. *Pestic. Sci.* **1983**, *14*, 444–448.
- (94) Kraljić, I.; Sharpatyi, V. A. Determination of singlet oxygen rate constants in aqueous solutions. *Photochem. Photobiol.* **1978**, 28, 583–586.
- (95) Sysak, P. K.; Foote, C. S.; Ching, T.-Y. Chemistry of singlet oxygen—XXV. Photooxygenation of methionine*. *Photochem. Photobiol.* **1977**, 26, 19–27.
- (96) Apell, J. N.; Pflug, N. C.; McNeill, K. Photodegradation of fludioxonil and other pyrroles: The importance of indirect photodegradation for understanding environmental fate and photoproduct formation. *Environ. Sci. Technol.* **2019**, *53*, 11240–11250.
- (97) Lion, Y.; Gandin, E.; Van de Vorst, A. On the production of Nitroxide radicals by singlet oxygen reaction: An epr study. *Photochem. Photobiol.* **1980**, *31*, 305–309.
- (98) Yoshimura, A.; Ohno, T. Lumiflavin-sensitized photooxygenation of indole. *Photochem. Photobiol.* **1988**, 48, 561–565.
- (99) Darmanyan, A. P.; Jenks, W. S.; Jardon, P. Charge-transfer quenching of singlet oxygen $O_2(^1\Delta_g)$ by amines and aromatic hydrocarbons. *J. Phys. Chem. A* **1998**, *102*, 7420–7426.
- (100) Scandola, F.; Balzani, V.; Schuster, G. B. Free-energy relationships for reversible and irreversible electron-transfer processes. *J. Am. Chem. Soc.* **1981**, *103*, 2519–2523.
- (101) Reed, A. E.; Weinstock, R. B.; Weinhold, F. Natural population analysis. J. Chem. Phys. 1985, 83, 735–746.
- (102) Shorter, J. Correlation Analysis of Organic Reactivity, with Particular Reference to Multiple Regression; Research Studies Press: Chichester, 1982; p xi, 235 p.
- (103) Exner, O. Correlation Analysis of Chemical Data; Springer, 1988.

- (104) Karelson, M. Molecular Descriptors in QSAR/QSPR; John Wiley & Sons, Inc.: New York, 2000.
- (105) Erickson, P. R.; Walpen, N.; Guerard, J. J.; Eustis, S. N.; Arey, J. S.; McNeill, K. Controlling Factors in the Rates of Oxidation of Anilines and Phenols by Triplet Methylene Blue in Aqueous Solution. *J. Phys. Chem. A* **2015**, *119*, 3233–3243.
- (106) Tsuji, Y.; Toteva, M. M.; Garth, H. A.; Richard, J. P. Kinetic and thermodynamic barriers to carbon and oxygen alkylation of phenol and phenoxide ion by the 1-(4-methoxyphenyl)ethyl carbocation. *J. Am. Chem. Soc.* **2003**, *125*, 15455–15465.
- (107) Zeinali, N.; Oluwoye, I.; Altarawneh, M.; Dlugogorski, B. Z. Kinetics of Photo-Oxidation of Oxazole and its Substituents by Singlet Oxygen. *Sci. Rep.* **2020**, *10*, No. 3668.
- (108) Braun, A. M.; Dahn, H.; Gassmann, E.; Gerothanassis, I.; Jakob, L.; Kateva, J.; Martinez, C. G.; Oliveros, E. (2+4)-Cycloaddition with Singlet Oxygen. 17O-Investigation of the Reactivity of Furfuryl Alcohol Endoperoxide. *Photochem. Photobiol.* **1999**, 70, 868–874
- (109) Manring, L. E.; Foote, C. S. Chemistry of singlet oxygen. 37. One-electron oxidation of tetramethylphenylenediamine by singlet oxygen. *J. Phys. Chem. C* **1982**, *86*, 1257–1259.
- (110) Potashnik, R.; Ottolenghi, M.; Bensasson, R. Photoionization and delayed fluorescence in liquid solutions of N,N,N,'N'-tetramethylp-phenylenediamine. *J. Phys. Chem. D* **1969**, *73*, 1912–1918.
- (111) Dixon, S. R.; Wells, C. H. J. Dye-sensitised photo-oxidation of 2-dimethylamino-5,6- dimethylpyrimidin-4-01 in aqueous solution. *Pestic. Sci.* **1983**, *14*, 444–448.
- (112) Clennan, E. L. Persulfoxide: Key intermediate in reactions of singlet oxygen with sulfides. *Acc. Chem. Res.* **2001**, *34*, 875–884.
- (113) Liu, F.; Liu, J. Oxidation Dynamics of Methionine with Singlet Oxygen: Effects of Methionine Ionization and Microsolvation. *J. Phys. Chem. B* **2015**, *119*, 8001–8012.
- (114) Méndez-Hurtado, J.; López, R.; Suárez, D.; Menéndez, M. I. Theoretical Study of the Oxidation of Histidine by Singlet Oxygen. *Chem. Eur. J.* **2012**, *18*, 8437–8447.
- (115) Kraljic, I.; Kramer, H. E. A. On the reaction of singlet molecular oxygen with N-allylthiourea in aqueous solution. *Photochem. Photobiol.* **1978**, *27*, 9–12.
- (116) Lightner, D. A.; Bisacchi, G. S.; Norris, R. D. On the mechanism of the sensitized photooxygenation of pyrroles. *J. Am. Chem. Soc.* **1976**, *98*, 802–807.
- (117) Quistad, G. B.; Lightner, D. A. On the photo-oxidation of 3,4-diethyl-2-methylpyrrole. *Tetrahedron Lett.* 1971, 12, 4417–4420.
- (118) Foote, C. S.; Clennan, E. L. Properties and Reactions of Singlet Dioxygen. In *Active Oxygen in Chemistry*; Foote, C. S.; Valentine, J. S.; Greenberg, A.; Liebman, J. F., Eds.; Springer: Dordrecht, 1995; pp 105–140.
- (119) Ogryzlo, E. A.; Tang, C. W. Quenching of oxygen by amines. *J. Am. Chem. Soc.* **1970**, 92, 5034–5036.
- (120) Miskosky, S.; Bertolotti, S. G.; García, N. A.; Argüello, G. A. On the $O_2(^1\Delta_g)$ -mediated photooxidative behaviour of tripeptide glycyl-tyrosyl-alanine in alkaline medium. A kinetic study. *Amino Acids* 1993, 4, 101–110.